Phase Modulation of Intense Ultrashort Laser Pulses Reflected From Steep, Dense Plasmas

R. J. Kingham,* P. Gibbon, W. Theobald, L. Veisz, and R. Sauerbrey
Insitut für Optik und Quantenelektronik, Friedrich-Schiller Universität, Jena, Germany
(Received 7 July 2000)

The phase modulation of intense ($I = 10^{18}$ W/cm^2) ultrashort laser pulses ($\tau_p = 70$ fs) after reflection from steep, dense plasmas has been temporally resolved for the first time in particle-in-cell simulations. The position of the turning point from where the pulse reflects has been compared to the phase modulation, over a range of angles of incidence. At normal incidence or s polarization the phase modulation almost exactly represents the movement of the turning point due to the light pressure. As the angle of incidence is increased for p polarization, the simple Fresnel relationship between phase modulation and displacement of the reflection position, $\Delta\phi(t) = -2k_0\Delta x(t)\cos\theta_0$, increasingly breaks down.

DOI: 10.1103/PhysRevLett.86.810 PACS numbers: 52.38.–r, 52.27.Ny, 52.65.Rr, 52.70.Kz

In recent years experimental techniques have been developed which allow fs-resolved phase measurements of ultrashort laser pulses. Frequency resolved optical gating (FROG) [1] has successfully been used to temporally resolve the electric field amplitude and phase modulation of individual, sub-200-fs, intense ($I \sim 10^{18}$ W/cm^2) pulses after interaction with an underdense plasma [2,3] and after reflection from a solid density plasma [4]. Frequency-domain interferometry (FDI) [5] has been utilized to both spatially and temporally resolve the phase shift of a probe pulse after reflection from a dense plasma created by a separate, intense, pump pulse. Formerly a multishot technique, FDI is currently being improved to work in "single shot" mode, too [6]. At intensities of $\sim 10^{18}$ W/cm^2 and above it becomes possible for the laser pulse to actually push solid density plasma since the light pressure $P_L = (1 + R)I/c$ (R is the plasma reflectivity) can exceed the plasma thermal pressure $P_{th} = n_e k_B T_e$, where n_e, T_e, and k_B are the plasma electron number density and temperature, and Boltzmann's constant, respectively. Very large accelerations are expected for ultraintense fs laser-solid plasma interactions [4,7]. To date, several experiments have been performed to measure things such as the density scale length at the critical density ($n_{cr} = \omega_0^2 m_{eo}\epsilon_0/e^2$ defines the electron critical density, where ω_0 is the laser angular frequency) and the plasma expansion velocity and motion using methods such as Doppler shifts of reflected probe pulses [8], resonance absorption profile spectroscopy [9] and FDI [5]. The latter techniques rely upon comparison with models and thus indirectly infer the scale length and plasma motion. Doppler shifts are not always a reliable, unambiguous source of the expansion velocity especially at high accelerations and when the reflectivity is highly time dependent [7]. Direct phase resolved measurements are more appropriate for probing the motion of fs-laser-produced plasmas *if one knows how the phase modulation relates to the reflection point position.*

Here we report on 1d3v (1 spatial dimension and 3 velocity dimensions) particle-in-cell (PIC) simulations of high-intensity, 70 fs long pulses reflecting from steep scale-length, overdense, collisionless plasmas. In particular, we have temporally resolved the phase modulation incurred upon reflection—*the first time this has been achieved in a PIC code* to the authors' knowledge. This has allowed us to check whether the phase modulation does indeed accurately represent the motion of the plasma as it is pushed by the laser pulse. We have also compared this with the phase modulation obtained via the Helmholtz equation. By varying the angle of incidence and polarization, we have found that the Fresnel result,

$$\Delta\phi(t) = -2k_0\Delta x_{tp}(t)\cos\theta_0\,, \tag{1}$$

holds true only at normal incidence or for s polarization but not for p polarization. $\Delta\phi$, Δx_{tp}, k_0, and θ_0 are the phase modulation, displacement of the turning/reflection point, wave number of the incident light, and angle of incidence, respectively. This is of paramount importance for all phase sensitive experiments utilizing fs, high contrast laser pulses, carried out with the intention of directly resolving the plasma motion. When Eq. (1) does not hold, sophisticated calculations and complicated experiments involving multiple diagnostics are required to "unravel" the various contributions to the phase modulation, such as the movement of the turning point and changes in the optical path length through the underdense plasma.

The 1d3v boosted electromagnetic (EM) PIC code BOPS [10,11] was used to model a system comprised of an exponential density ramp of scale length $L = \lambda_0/10$ and length $k_0 x_{\text{ramp}} = 20$ leading up to an overdense, uniform plasma slab of density $n_{eo} = 10 n_{cr}$ and extent $k_0 x_{\text{slab}} = 2.5$ or longer. At the start of the simulation the electron and ion temperatures were set to $T_e = 2$ keV and $T_i = 200$ eV. For the results presented here 2^{18} electrons and 2^{18} (mobile) ions with $m_i/Zm_e = 3672$ (i.e., $A/Z = 2$) were used. A short, intense, unchirped Gaussian pulse, $E_i(t) = E_0 \exp(-t^2/2t_p^2)\cos\omega_0 t$, of peak intensity $I = 10^{18}$ W/cm^2 was injected into the simulation box through the vacuum boundary at θ_0 degrees to the target normal. The reflected pulse $E_r(t)$ returning through this boundary at a later time was recorded. Even though there is only one spatial dimension BOPS can

 0031-9007/01/86(5)/810(4)$15.00

model arbitrary angles of incidence by using the Lorentz boost technique [11]. The grid point spacing Δx ranged from $\lambda_0/320$ at 0° to $\lambda_0/470$ at 60° which ensured that the Debye length was always resolved in the boost frame. To make sure that the EM absorbing boundary functioned correctly, a substantial region of vacuum of length $k_0 x_{\text{vac}} = 20$ was set up before the start of the ramp.

The evolution of the electron density profile $n_e(x)$ over the course of the simulation is presented in Fig. 1 for 30° angle of incidence. The time $\omega_0 t = 0$ corresponds to the arrival of the peak of the pulse at $k_0 x = 0$, the turning point on the initial plasma profile. For s polarization (upper plot) the plasma initially expands slightly into the vacuum. Then for $-200 < \omega_0 t < 200$ the electrons in the vicinity of the turning point are pushed into the denser plasma by the $v \times B$ force of laser pulse and the ions are subsequently dragged along. During the interaction the density ramp is steepened and x_{tp}, the position where $n_e(x) = n_{tp} = n_{cr} \cos^2\theta_0$, ends up being pushed about $\lambda_0/6$ into the denser plasma (see *solid black* curve).

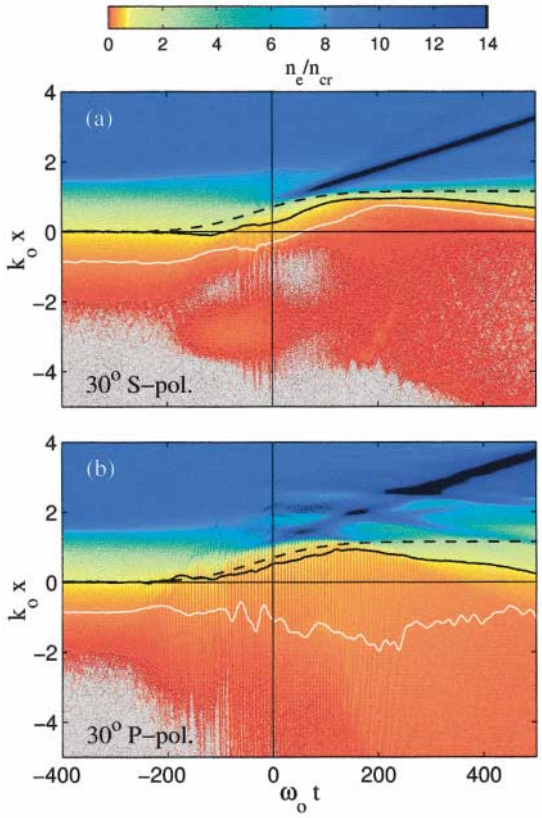

FIG. 1 (color). Evolution of the electron density profile $n_e(x)$ during the simulation for (a) 30° s and (b) 30° p polarization. A vertical slice through each plot corresponds to a "snapshot" of $n_e(x)$. The color represents the value of n_e (see scale above). The extensive grey regions correspond to $n_e < 0.02 n_{cr}$. Places on the profile where n_e equals n_{tp} (turning point density) and $n_{tp}/4$ are denoted by the *solid* black and white curves, respectively. The overlaid dashed black curve depicts the hole-boring estimate of how the laser pulse pushes the plasma.

After the laser pulse the density ramp relaxes back into the vacuum.

The situation is somewhat different for p polarization. While the laser still pushes the overdense plasma in a way similar to s polarization, the dynamics of the underdense plasma is totally different. For p polarization an underdense shelf [12] is formed which grows during the laser interaction. Conversely the s-polarized pulse pushes all the electrons [in a layer approximately $\lambda_0/(4\cos\theta_0)$ thick] just before the turning point. For p polarization there is a component of the electric field along the density gradient in addition to the $v \times B$ force. This E-field changes sign over one optical cycle unlike $v \times B$ (which oscillates at $2\omega_0$). The surface electrons oscillating in this field are known to be responsible for the enhanced laser absorption at p polarization (e.g., "Brunel heating" [13]) and underdense ion shelf formation [14]. To emphasize the difference between the dynamics of the underdense plasma for s and p polarizations, the location of $n_e(x) = n_{tp}/4$ is highlighted by *white* curves (which are cycle averaged). Other notable features in Fig. 1 include (i) cavitation in the underdense plasma for s polarization during $-200 < \omega_0 t < 100$, (ii) electrons following the ions reflected off the laser-plasma interface into the bulk plasma (dark diagonal feature, starting at $\omega_0 t \sim 0$), (iii) high frequency oscillations of the electron density profile between $\omega_0 t = -200$ and 200, and (iv) fast electrons (generated at critical) streaming into the bulk plasma (especially prominent for p polarization between $-150 < \omega_0 t < 150$).

The dashed curves in Fig. 1 show an estimate of how far the plasma is pushed. It was obtained using the so called hole-boring velocity [15]

$$\frac{V_{hb}}{c} = \sqrt{\cos\theta_0 \left(\frac{I_{18}\lambda_\mu^2}{2.75}\right)\left(\frac{n_{cr}}{n_e}\right)\left(\frac{Z}{A}\right)\frac{m_{eo}}{m_p}} \qquad (2)$$

(where $I_{18} = I/10^{18}$ W/cm^2 and $\lambda_\mu = \lambda_0/1\ \mu$m) which is derived using simple time averaged photon-ion momentum balance considerations. We assumed that hole-boring started at $x = x_{tp}$ and subsequently pushed further up the initial, exponential density profile. It is remarkable how well the hole-boring estimate agrees with the maximum displacement of n_{tp} from the PIC simulation at $\omega_0 t \sim 150$, considering how few optical cycles are in the pulse (only 27). The discrepancy for later times simply arises because relaxation of the plasma into the vacuum is not included in the hole-boring estimate. It is worth noting that plasma is pushed the order of 100 nm at an intensity of 10^{18} W/cm^2 and a pulse length of 100 fs. In real 3D geometry where the intensity at the center of the focal spot is greatest, the surface will also be pushed in the most at the center thus creating a depression/dimple. But even for tight focusing to a radius of about 3 μm, the steepest surface deformation is only on the order of 3°. Thus a 1D treatment is appropriate under the conditions in this investigation.

The time resolved phase modulation imprinted on the reflected pulse during its interaction with the plasma was obtained from the PIC simulation as follows. First the analytic signal $E_c(t) = E_r(t) - \imath E_{Hi}(t)$ corresponding to the real valued E-field $E_r(t)$ was calculated, where $E_{Hi}(t) = -(\pi t)^{-1} * E_r(t)$ is the Hilbert transform of $E_r(t)$ [16]. The complex-valued analytic signal permits extraction of the phase $\phi(t)$ and amplitude $|E(t)|$. Before phase extraction, $E_c(t)$ was filtered using a Gaussian frequency band-pass filter, $F(\omega) = \exp[-(\omega - \omega_c)^2/2\Delta\omega^2]$, centered at $\omega_c = \omega_0$ and of width $\Delta\omega/\omega_0 = 2/\pi^2$. The phase was then extracted, unwrapped, and finally the carrier phase $\omega_0 t$ was subtracted to leave the time resolved phase modulation, $\Delta\phi(t)$. Filtering removes the harmonics $\omega_n = n\omega_0$ (for $n > 1$) that are produced when a high intensity laser pulse interacts with a steep, highly overdense plasma [17]. These harmonics cause oscillations in $\Delta\phi(t)$ which are not of interest here. After filtering only the secular variation arising from the fundamental is left.

We find that the phase modulation in the reflected pulse faithfully reproduces $\Delta x_{tp}(t)$ at 0° and 30° s polarization but not at 30° p polarization as demonstrated in Fig. 2. The phase modulation (solid curves, no symbols) has been converted to the equivalent mirror displacement $\Delta x_\phi = -\Delta\phi/2k_0\cos\theta_0$, and aligned with Δx_{tp} at $\omega_0 t = -300$. The Δx_{tp} curves (black squares) have been time averaged, also using the Gaussian frequency band-pass filter with $\omega_c = 0$, to remove the high frequency oscillations thereby allowing easier comparison with the phase. Furthermore, Fig. 2 shows that the discrepancy between $\Delta x_\phi(t)$ and $\Delta x_{tp}(t)$ grows as the angle of incidence is increased. At 45° the discrepancy is arguably the worst of the 5 values of θ_0 simulated. For the 0° and 60° simulations $A/Z = 1.9$ rather than 2. Fresnel reflection breaks down for p polarization because of the underdense shelf that forms during the laser-plasma interaction. The optical path length before the turning point steadily *decreases* with time (i.e., plasma refractive index is less than 1) as the underdense shelf evolves and counteracts the path length increase due to the recession of the reflection point. Conversely for s polarization or at normal incidence $\Delta\phi(t)$ is dominated by the movement of the turning point and Fresnel reflection is valid. In principle relativistic laser-pulse propagation effects could also cause a departure from Eq. (1) at high intensities. Relativistic phase modulation in the underdense plasma and relativistic induced transparency [where n_{cr} is increased by a factor $\gamma = \sqrt{1 + (eE/m_{eo}\omega_0 c)^2}$] are two such effects. The intensity used here (for which $\gamma \approx 1.1$) is not yet high enough for relativistic effects to play an important role.

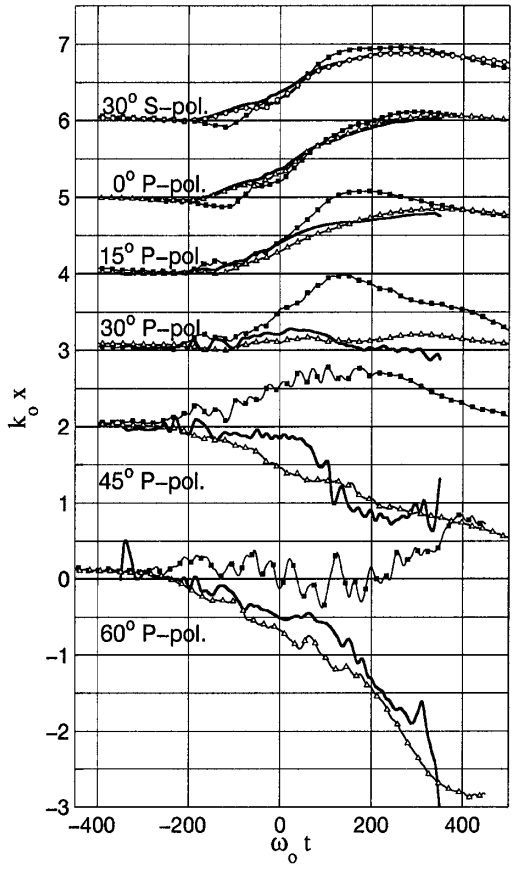

FIG. 2. Comparison of the PIC code phase modulation (solid curves) with the electron density turning point (black squares) for a selection of angles. The postprocessed Helmholtz phase modulation is depicted by white triangles (p polarization) and white circles (s polarization).

In order to check that the departure from Fresnel reflection for p polarization does arise from the changing optical path length through the underdense shelf, the PIC density profiles were postprocessed using Helmholtz solvers. The Helmholtz equation describes the propagation of a constant amplitude light wave in a fixed, underdense plasma profile (or other optical medium) up to the turning point. At regular time intervals (e.g., 10 times per cycle) the Helmholtz equation was solved for the E-field (or B-field) standing wave pattern in the instantaneous PIC $n_e(x)$ profile. The phase difference between the incident and reflected waves (at the vacuum boundary) was then extracted. The phase modulation obtained by this method is shown in Fig. 2 (as the equivalent mirror displacement) via the curves with white symbols. The correspondence between these Helmholtz postprocessed $\Delta x_\phi(t)$ curves and their PIC counterparts is almost perfect for s polarization and $\theta_0 = 0°$ and very good for p polarization at 15° and 30°. This lends considerable confidence to the method described here for extracting phase modulation from 1D-PIC codes. At 45° and 60° p polarization the Helmholtz phase curves broadly follow the PIC phase rather than $\Delta x_{tp}(t)$. Our s- and p-polarization solvers are based on those of Rae and Burnett [18]. To phenomenologically model resonance absorption at p polarization the solvers incorporate spatial dispersion $\nu_d = \sqrt{eE_d/m_{eo}L}$ in the vicinity of the resonance point and iteratively solve for the EM fields. E_d is the E-field at $\epsilon \approx 0$ and L is the density

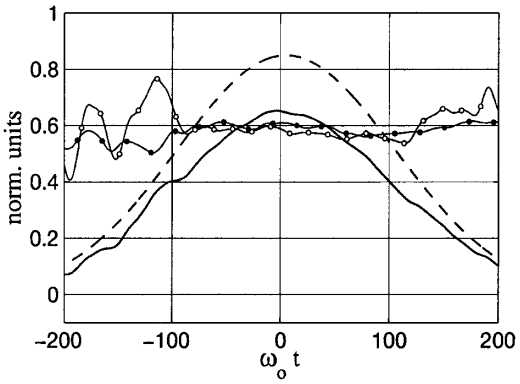

FIG. 3. E-field envelopes $|E|$ for the incident (dashed curve) and reflected (solid curve) PIC laser pulse at 30° angle of incidence and p polarization. The corresponding time resolved reflectivity, $R = |E_r|^2/|E_i|^2$, is depicted by the curve with white circles. Curves with black circles represent the reflectivity obtained via postprocessing with a Helmholtz solver.

scale length. When the s-polarization solver is used on the p-polarization PIC density profiles the resulting phase modulation curves are almost identical to those shown in Fig. 2, which were obtained using the p-polarization solver. This corroborates the fact that the (temporally changing) optical path length reduction in the underdense shelf is primarily responsible for the departure from Fresnel reflection for p polarization.

So far we have concentrated on the phase modulation effect, but the phase extraction method also yields the E-field amplitude. In Fig. 3 $|E_i(t)|$ and $|E_r(t)|$, the incident (dashed line) and reflected (solid line) E-field amplitudes from the PIC simulation, respectively, are shown for the 30° p-polarization simulation. The time resolved reflectivity $R = |E_r(t)|^2/|E_i(t)|^2$ obtained directly from the PIC code (curve with white circles) and from the Helmholtz postprocessing technique described above (black circles) are also depicted. The reflectivities agree almost exactly over the center of the pulse when $\nu_d(x)$ is reduced to $0.1\sqrt{eE_d(x)/m_{eo}L(x)}$. We used this calibrated value of the phenomenological spatial dispersion for calculating all the Helmholtz phase curves in Fig. 2. The excellent agreement between PIC and Helmholtz reflectivity is a further indication that the Helmholtz postprocessing technique works well.

In summary, the phase modulation imprinted on an intense fs laser pulse during reflection from a short scale-length, overdense plasma has been temporally resolved in PIC simulations for a range of angles of incidence. The results have important ramifications for planned experiments that set out to directly temporally resolve overdense plasma motion with fs resolution using phase sensitive experimental techniques such as FROG. For normal incidence or for s polarization the Fresnel approximation, Eq. (1), holds very well for $L = \lambda_0/10$ and $n_{eo} = 10n_{cr}$. However, at oblique angles of incidence and p polarization we have found that $\Delta\phi(t) = -2k_0\Delta x_{tp}\cos\theta_0$ no longer holds due to the formation of an underdense shelf in the density profile which distorts the optical path length. We expect Fresnel reflection to still be valid for s but not p polarization at *shorter* scale lengths and higher densities. Conversely, the long scale-length profile (i.e., $L \gg \lambda_0/10$) caused by a laser prepulse implies movement away from the Fresnel regime (irrespective of polarization) and thus makes accurate reconstruction of plasma motion from reflected phase modulation much more difficult. It is therefore essential to use an s-polarized driving pulse or arrange for near-normal incidence. This ensures that the time resolved phase modulation gives a reliable measure of the movement of the reflection point under the influence of the intense laser pulse.

The authors thank Professor A. R. Bell for the use of workstations at the Plasma Physics Group, Imperial College, London. This work grew to fruition under the support of the SILASI and GAUSEX TMR networks.

*Current address: Plasma Physics Group, Imperial College, Blackett Laboratory, London SW7 2BZ, UK.

[1] R. Trebino and D. J. Kane, J. Opt. Soc. Am. A **10**, 1101 (1993).
[2] P. R. Bolton *et al.,* J. Opt. Soc. Am. B **13**, 336 (1996).
[3] S. P. Nikitin *et al.,* Opt. Commun. **157**, 139 (1998).
[4] R. Hässner *et al.,* in *Superstrong Fields in Plasma* (AIP, New York, 1998), p. 213.
[5] J. P. Geindre *et al.,* Opt. Lett. **19**, 1997 (1994).
[6] J. C. Gauthier and S. Rebibo (private communication).
[7] R. Sauerbrey, Phys. Plasmas **3**, 4712 (1996).
[8] H. M. Milchberg and R. R. Freeman, Phys. Rev. A **41**, 2211 (1990); O. L. Landen and W. E. Alley, Phys. Rev. A **46**, 5089 (1992); X. Liu and D. Umstadter, Phys. Rev. Lett. **69**, 1935 (1992).
[9] O. L. Landen, D. G. Stearns, and E. M. Campbell, Phys. Rev. Lett. **63**, 1475 (1989).
[10] P. Gibbon and A. R. Bell, Phys. Rev. Lett. **68**, 1535 (1992).
[11] P. Gibbon *et al.,* Phys. Plasmas **6**, 947 (1999).
[12] D. W. Forslund *et al.,* Phys. Rev. A **11**, 679 (1975).
[13] F. Brunel, Phys. Fluids **31**, 2714 (1988).
[14] P. Gibbon, Phys. Rev. Lett. **73**, 664 (1994).
[15] S. C. Wilks *et al.,* Phys. Rev. Lett. **69**, 1383 (1992).
[16] R. N. Bracewell, *The Fourier Transform and Its Applications* (McGraw-Hill, New York, 1978), 2nd ed., p. 267.
[17] P. Gibbon, IEEE J. Quantum Electron. **33**, 1915 (1997).
[18] S. C. Rae and K. Burnett, Phys. Rev. A **44**, 3835 (1991).